

## Accepted Manuscript

A three-drug nanoscale drug delivery system designed for preferential lymphatic uptake for the treatment of metastatic melanoma

Bhuvana S. Doddapaneni, Sergiy Kyryachenko, Sharmeen E. Chagani, Raid G. Alany, Deepa A. Rao, Arup K. Indra, Adam W.G. Alani

PII: S0168-3659(15)30224-8  
DOI: doi: [10.1016/j.jconrel.2015.11.013](https://doi.org/10.1016/j.jconrel.2015.11.013)  
Reference: COREL 7980

To appear in: *Journal of Controlled Release*

Received date: 16 July 2015  
Revised date: 18 October 2015  
Accepted date: 2 November 2015



Please cite this article as: Bhuvana S. Doddapaneni, Sergiy Kyryachenko, Sharmeen E. Chagani, Raid G. Alany, Deepa A. Rao, Arup K. Indra, Adam W.G. Alani, A three-drug nanoscale drug delivery system designed for preferential lymphatic uptake for the treatment of metastatic melanoma, *Journal of Controlled Release* (2015), doi: [10.1016/j.jconrel.2015.11.013](https://doi.org/10.1016/j.jconrel.2015.11.013)

This is a PDF file of an unedited manuscript that has been accepted for publication. As a service to our customers we are providing this early version of the manuscript. The manuscript will undergo copyediting, typesetting, and review of the resulting proof before it is published in its final form. Please note that during the production process errors may be discovered which could affect the content, and all legal disclaimers that apply to the journal pertain.

**A three-drug nanoscale drug delivery system designed for preferential lymphatic uptake  
for the treatment of metastatic melanoma**

Bhuvana S. Doddapaneni<sup>1</sup>, Sergiy Kyryachenko<sup>1</sup>, Sharmeen E. Chagani<sup>1</sup>, Raid G. Alany<sup>2</sup>, Deepa  
A. Rao<sup>3</sup>, Arup K. Indra<sup>1</sup>, Adam W. G. Alani<sup>1,\*</sup>

<sup>1</sup> Department of Pharmaceutical Sciences  
College of Pharmacy  
Oregon State University,  
Corvallis, OR, USA

<sup>2</sup> School of Pharmacy and Chemistry, Drug Discovery,  
Delivery and Patient Care (DDDPC) Theme  
Kingston University  
London, UK

<sup>3</sup> School of Pharmacy  
Pacific University  
Hillsboro, OR, USA

**\* CORRESPONDING AUTHOR**

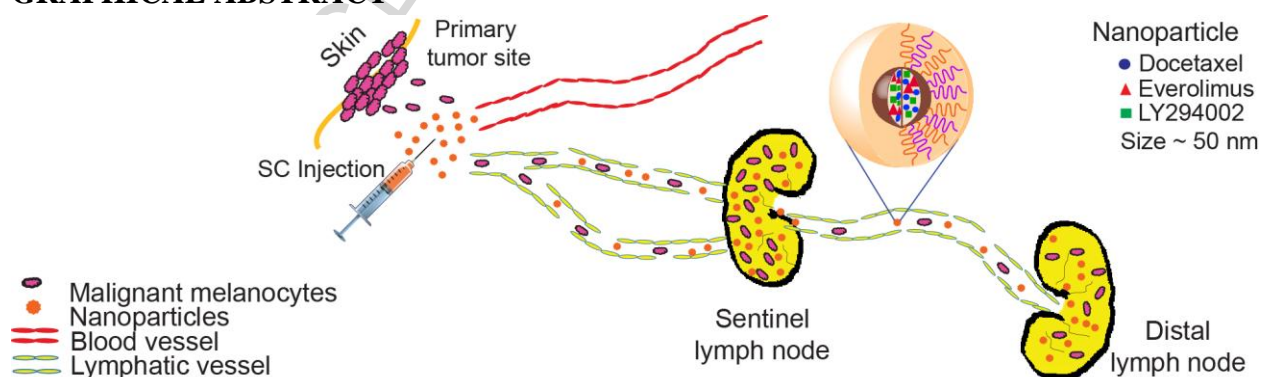
Adam W. G. Alani  
Assistant Professor of Pharmaceutics  
Department of Pharmaceutical Sciences  
College of Pharmacy  
Oregon State University-Oregon Health & Science University Affiliate Assistant Professor  
Department of Biomedical Engineering School of Medicine at Oregon Health & Science  
University Oregon State University-Portland Campus at OHSU  
2730 SW Moody Ave, CL5CP  
Portland Oregon 97201-5042

Tel: (503) 346-4702

Email: Adam.Alani@oregonstate.edu

**ABSTRACT**

Metastatic Melanoma has a high mortality rate due to lymphatic progression of the disease. Current treatment is surgery followed by radiation and intravenous chemotherapy. However, drawbacks for current chemotherapeutics lie in the fact that they develop resistance and do not achieve therapeutic concentrations in the lymphatic system. We hypothesize that a three-drug nanoscale drug delivery system, tailored for lymphatic uptake, administered subcutaneously, will have decreased drug resistance and therefore offer better therapeutic outcomes. We prepared and characterized nanoparticles (NP) with docetaxel, everolimus, and LY294002 in polyethyleneglycol-*block*-poly( $\epsilon$ -caprolactone) (PEG-PCL) polymer with different charge distributions by modifying the ratio of anionic and neutral end groups on the PEG block. These NP are similarly sized ( $\sim 48\text{nm}$ ), with neutral, partially charged, or fully charged surface. The NP are able to load  $\sim 2\text{mg/mL}$  of each drug and are stable for 24 h. The NP are assessed for safety and efficacy in two transgenic metastatic melanoma mouse models. All the NP were safe in both models based on general appearance, weight changes, death, and blood biochemical analyses. The partially charged NP are most effective in decreasing the number of melanocytes at both the proximal (sentinel) lymph node (LN) and the distal LN from the injection site. The neutral NP are efficacious at the proximal LN, while the fully charged NP have no effect on either LN. Thus, our data indicates that the NP surface charge and lymphatic efficacy are closely tied to each other and the partially charged NP have the highest potential in treating metastatic melanoma.

**GRAPHICAL ABSTRACT****KEYWORDS**

Melanoma treatment, lymphatic drug delivery, nanoparticles, combination therapy, melanoma transgenic mouse model

## INTRODUCTION

Melanoma is the deadliest form of skin cancer with a very high mortality rate.[1] The standard treatment for early stage diagnosis is surgical removal of the tumor and for late stage surgery followed by radiation and chemotherapy. Tumor metastasis is the major reason for high mortality rates in melanoma. The process begins with the detachment of tumor cells from the adjacent endothelial cells and the basement membrane and is accompanied by the secretion of various cytokines and growth factors. Migration through the lymphatic vasculature is preferred over blood vessels because of reduced flow rates and pressure, easier access to the vessel, and wider vessel lumens.[2] Up to 80% of melanomas metastasize through the lymphatic system.[3] Additionally, tumor cells secrete lymphangiogenic growth factors like Vascular Endothelial Growth Factors that can stimulate lymphangiogenesis and further promote lymphatic migration.[3] These enlarged lymphatic vessels act as a freeway for the metastatic cells to gain access and spread to distal lymph nodes (LN) and organs.

Extensive research over the past two decades has helped us elucidate the driver mutations occurring in different oncogenes involved in the development of metastatic melanoma. The majority studied mutations occur primarily in the BRAF (a serine/threonine protein kinase) genes and have approved targeted therapies for patients in stage IV or unresectable melanoma.[4, 5] However, newer emerging genetic targets include Neuroblastoma –Rat Sarcoma (NRAS)[4-6] and nuclear receptors like Retinoid X Receptor- $\alpha$  (RXR $\alpha$ ) genes.[7, 8] In pathological conditions, point mutations at the codon 61 of NRAS (NRAS<sup>Q61K</sup>) gene locks the activated form of NRAS-GTP thereby promoting continuous up regulation of downstream effector proteins and signaling pathways in the malignant melanoma phenotype.[9, 10] Activated NRAS<sup>Q61K</sup> mutations play a significant role in the development of metastatic melanoma and are the primary driver mutations that are responsible for the spread of the disease in humans.[11, 12] These oncogenic drivers in the NRAS<sup>Q61K</sup> promote invasiveness of the malignant cells and have larger nodal involvement when compared to the BRAF mutations.[13] RXR $\alpha$  plays a major role in gene expression and signal transduction and in human melanomas the expression of RXR $\alpha$  is lost as the disease progresses.[14] Animal studies have indicated that the loss of RXR $\alpha$  in skin keratinocytes can lead to the increased melanocyte proliferation and the formation of malignant melanomas.[8, 14] Thus, while therapies targeting the BRAF mutations exist, no such therapeutic approaches are currently available for the NRAS or RXR $\alpha$  mutations. In the current study, we have utilized two melanoma models (1) NRAS<sup>Q61K</sup> mice with functional RXR $\alpha$  and activated NRAS in the melanocytes [11], and (2) bigenic NRAS<sup>Q61K</sup> | RXR $\alpha$ <sup>ep-/-</sup> mice selectively lacking RXR $\alpha$  in epidermal keratinocytes in combination with the activated NRAS. Ablation of RXR $\alpha$  alongside with NRAS<sup>Q61K</sup> mutations resulted in increased number/size of spontaneous melanomas with reduced latency and increased invasion to draining lymph nodes in the NRAS<sup>Q61K</sup> | RXR $\alpha$ <sup>ep-/-</sup> mice.[15]

Currently the FDA has 10 approved drugs for the treatment of metastatic melanoma based on inhibiting BRAF, mitogen-activated protein kinase, tyrosine kinase, or angiogenesis.[16, 17] The major drawback of the current therapy is the inability to deliver therapeutic concentrations to the lymphatic system while avoiding systemic toxicity. The majority of these inhibitors are administered intravenously (IV), resulting in high doses in the systemic circulation with an insufficient dose reaching the lymphatic vasculature. Secondly, chemoresistance has been noted for the approved drugs when used individually.[18] Tumor cells are also known to induce resistance by up regulating alternate pathways when one of the pathways is blocked by specific inhibitors.[18] Thus, there is a need for a combination therapy that can overcome drug resistance by acting on multiple pathways involved in melanoma as well as a drug delivery system that can be delivered into the lymphatic system.

Molecules and/or drug delivery systems accumulate in the lymphatics based on molecular weight, size, surface charge, and site of administration.[19, 20] A direct correlation between lymphatic absorption and molecular weight indicates that molecules with MW > 16,000 Da preferentially accumulate into the lymphatics,[21] while, the optimum particle size for lymphatic uptake is between 10-80 nm.[22] Anionic charged particles have higher uptake compared to cationic or neutral particles, possibly due to the slight negative charge of the interstitium at the site of injection.[23] The site of administration also plays a major role in delivering therapeutic payloads to the lymphatics where a higher accumulation of injected formulation in lymphatics is noted when injected subcutaneously (SC) as compared to the IV.[24] Any macromolecules or nanoscale drug delivery systems injected IV are limited to the vascular space and do not partition into the interstitium. Thus, their uptake into the lymphatics is limited.[22, 25] As most chemotherapeutics for the treatment of melanoma are small molecules without the necessary properties for lymphatic uptake, a drug delivery system is needed to achieve the necessary lymphatic accumulation.

Chemotherapeutics like docetaxel (DTX; PubChem CID: 148124), everolimus (EVR; PubChem CID: 6442177), and the experimental compound LY294002 (LY; PubChem CID: 3973) are small molecules with MW ranging from 300 to a 1000 Da with low intrinsic aqueous solubilities (Figure 2a). Each of these molecules acts on different pathways to inhibit tumor proliferation. DTX acts by stabilizing the microtubules, EVR and LY act on mammalian target of rapamycin, mTORC1 and mTORC2, respectively.[26-28] Together, EVR and LY, can completely inhibit the mTOR pathway while LY is also capable of inhibiting the Phosphoinositide 3-Kinase (PI3K) pathway.[27, 28] However, IV or SC administration of these molecules individually or together will lead to systemic absorption with little accumulation in the lymphatic system.

Nanoparticles (NP), prepared with amphiphilic block copolymers, are drug delivery systems that can be modified to target the lymphatic system.[29] These block copolymers are comprised of hydrophilic and hydrophobic domains with varying chain lengths and different end groups that

can be used to modulate NP size and charge density.[30] Additionally, polyester-based polymers like polyethylene glycol-*block*-poly( $\epsilon$ -caprolactone) (PEG-PCL) are biodegradable and biocompatible.[30] The NP formulated using these polymers have demonstrated excellent stability, increase the drug circulation time, and are capable of solubilizing poorly water soluble drugs while simultaneously delivering multiple drugs.[30-32] Incorporation of DTX, EVR, and LY into a NP drug delivery system might overcome the chemoresistance issues while simultaneously targeting the lymphatics. Therefore, we hypothesize that DTX, EVR, and LY loaded PEG-PCL NP with specific size and surface charge density, administered SC, will have preferential uptake and accumulation in the lymphatic system and will exert synergistic anti-proliferative effects in clinically relevant melanoma models. Our objectives are to formulate and characterize three-drug loaded NP for the co-delivery of DTX, EVR and LY, and establish to their safety and efficacy in relevant melanoma mouse models.

## MATERIALS AND METHODS

### Materials

The polymers, methoxy poly(ethylene glycol)-*block*-poly( $\epsilon$ -caprolactone) (mPEG<sub>5000</sub>-*b*-PCL<sub>10000</sub>) [Mn=15000; PDI = 1.17] and carboxy poly(ethylene glycol)-*block*-poly( $\epsilon$ -caprolactone) COOH-PEG<sub>5000</sub>-*b*-PCL<sub>10300</sub> [Mn=15300; PDI=1.39] were purchased from Advanced Polymer Materials Inc. (Montreal, CAN). DTX, EVR and LY were purchased from LC laboratories (Woburn, MA). Slide-A-Lyzer™ Dialysis Cassettes, 20K MWCO were obtained from Thermo Scientific Inc (Fairlawn, NJ). A375 human melanoma epithelial cells were obtained from American Type Culture Collection (Manassas, VA). Two metastatic melanoma mice models, *Tyr NRAS<sup>Q61K</sup> RXR $\alpha$ <sup>L2/L2</sup>* and *Tyr NRAS<sup>Q61K</sup> RXR $\alpha$ <sup>ep-/-</sup>*, were generated according to previous work.[8, 11, 15, 33] CellTiter-Blue® Cell viability Assay was obtained from Promega Inc. (Madison, WI). Fontana-Masson stain kit was purchased from American Mastertech Scientific, Inc. (Lodi, CA). All reagents and supplies were purchased from VWR International, LLC (Radnor, PA) or Fischer Scientific Inc. (Fairlawn, NJ).

### Methods

#### *Preparation and characterization of three-drug loaded nanoparticles*

DTX, EVR and LY three-drug loaded NP were prepared using a solvent evaporation method.[34] Briefly, 40 mg of the PEG-PCL polymers at various concentrations were dissolved in 2 mL of acetone. For neutral NP only mPEG-PCL (neutral NP) was used, while for partially charged NP, a mixture of mPEG: COOHPEG (60:40) (partially charged NP) with PCL was used. For the fully charged NP, 100% COOHPEG-PCL (fully charged NP) was used. Stock solutions of DTX, EVR and LY in acetone were prepared and required concentrations were added to the polymer solution to achieve a final concentration of 2 mg/mL of each drug. The drug polymer solution was transferred into a 10 mL round bottom flask and normal saline, 2 mL, was added

followed by removal of the organic solvent using a rotary evaporator. The evaporation cycle was divided into three segments, with the first segment lasting 7 min at 420 mbar, the second for 7 min at 320 mbar and the final segment of 6 min at 200 mbar. The temperature of the water bath was maintained at 45 °C with a rotation of 100 rpm for the round bottom flask. To ensure complete removal of acetone the nanoparticle suspension placed in a hood for an additional hour to allow for evaporation of any residual acetone. Under these conditions minimal evaporation of normal saline occurs. The final volume was adjusted to 2 mL with saline. The NP were collected in a centrifuge tube and spun at 5,000 rpm for 3 minutes and filtered/sterilized using a 0.2 µm nylon filter prior to use.

NP were characterized for size, surface charge distribution, and drug loading. Particle size was characterized by Dynamic Light Scattering (DLS) using a Malvern Nano ZS (Malvern Instruments Inc, U.K.). All measurements were performed in triplicate and data is presented as the mean z-average diameter  $\pm$  SD (nm) and polydispersity index (PDI  $\pm$  SD). Statistical analysis (one way ANOVA) was performed using Graph Pad Prism software to determine statistical significance between the sizes of the empty, partially charged, and fully charged NP. The surface charge was measured using the same instrument and the data of three replicates is presented as mean zeta potential ( $\zeta$ )  $\pm$  SD (mV). The drug loading was determined by reverse phase high performance liquid chromatography (RP-HPLC) using a Shimadzu HPLC system consisting of LC-20 AT pump and SPD M20 a diode array detector. The analysis was performed using Zorbax C8 Column (4.6×75 mm, 3.5 µm) in isocratic mode with acetonitrile/water (62/38) containing 0.1% phosphoric acid and 1% methanol at a flow rate of 1 mL/min and an injection volume of 10 µL. Column temperature was maintained at 40 °C. The DTX, LY, and EVR peaks were monitored at 227 nm, 303nm and 279 nm respectively at retention times of 1.7, 2.3 and 5.7 min respectively. The peak purity for each of the compounds was determined at its respective wavelength using the Shimadzu LC Solutions software and based on the peak purity indices for all three compounds of 1.000 no impurities for the three peaks were detected (please refer to the supplemental information section for a more detailed discussion of the peak purity). The log P values for DTX, LY, and EVR are 3.54, 3.33, and 5.9 respectively (Advanced Chemistry Development ACD/Universal LogD Module, Percepta 14.0.0 (Build 1996)). The log D at pH 7.4 for DTX, LY, and EVR are 3.54, 3.33, and 4.25 (Advanced Chemistry Development ACD/Universal LogD Module, Percepta 14.0.0 (Build 1996)). Given the similarity in the log P and log D at pH 7.4 for DTX and LY the retention times for both molecules on the RP-HPLC are within 0.6 min of each other. All measurements were performed in triplicate and loading data are presented as mean drug loading (mg/mL)  $\pm$  SD. As part of the RP-HPLC quantification residual acetone content was also assessed as a quality control measure and residual acetone content in the nanoparticles was determined to be 11.2  $\pm$  3.6 mg per day, which is well below the United States Pharmacopeia 30 chapter <497> stated limit for a class 3 organic solvent of 50 mg per day.

### *In vitro drug release from the nanoparticles*

The three-drug NP were prepared as described above. The release profile of DTX, EVR, and LY from neutral, partially charged, and fully charged NP was evaluated in 10 mM acetate buffer at pH 5.0 and 10 mM phosphate buffer pH 7.4 at 37 °C over 168 h (1 week) under sink conditions by dialysis.[35] Briefly, in three separate dialysis cassettes, for each type of NP, 2.0 mL of the sample was loaded. A MWCO of 20,000 Da was chosen to enable the unhindered diffusion of free drugs along with the unassociated polymer molecules out of the cassette. The cassettes were placed in 2.5 L of acetate or phosphate buffer and the temperature was maintained at 37 °C for the duration of the experiment. Sink conditions were ensured by changing the buffer every 3 h. Samples of 20 µL were withdrawn at 0, 0.5, 1, 2, 3, 6, 12, 24, 48, 72, 96, 120, 144, and 168 h and were replaced with an equal volume of fresh buffer. Samples were diluted 50 fold in the mobile phase and analyzed by RP-HPLC for drug content. The data is presented as mean % drug release  $\pm$  SD. Data were curve fitted using a two phase exponential association equation in Graph Pad Prism 5 software. The time required to release 50% of the drug ( $t_{1/2}$ ) in two phases, fast and slow, and the goodness of fit ( $r^2$ ) values of three replicates are presented. Statistical Analysis using one-way ANOVA with Tukey's post-test was performed on the release profiles for each drug across the different NP to assess for differences in rates of drug release. Statistical analysis was performed using GraphPad Prism 5 software.

#### ***In vitro cell viability assay and combination index (CI) analysis***

A375 human malignant epithelial melanoma cells were seeded at a density of 5,000 cells/well in 96 well plates and allowed to attach for 12 h at 37 °C. Post-attachment, cells were treated with individual drugs (DTX, EVR, or LY) or two drugs (DTX:EVR, DTX:LY, or EVR:LY) or three drugs (DTX:EVR:LY) dissolved in DMSO at equivalent molar ratios. The concentration range for all three drugs was between 0.01–10,000 nM. The final concentration of DMSO in the wells was 1%. Empty NP and three drug loaded NP cell viability studies were also conducted under similar conditions. Cell viability was determined after 72 h by treatment with 20 µL of CellTiter-Blue<sup>®</sup> reagent followed by one hour of incubation at 37 °C and fluorescence intensity ( $560_{EX}/590_{EM}$ ) was measured. All measurements were performed in quadruplicate. The mean drug concentration at 50% growth inhibition ( $IC_{50}$ ) was determined using nonlinear fitting using a log(inhibitor) vs response – variable slope equation in GraphPad Prism (version 5.00 for Windows, GraphPad Software, San Diego California USA). For combinations in DMSO, the concentrations are reported for the most potent drug, usually DTX, except for the EVR:LY group, where they are reported in terms of EVR concentration for direct comparison. The combination effect of DTX:EVR, DTX:LY, EVR:LY, and DTX:EVR:LY in DMSO in A375 cells was evaluated using Compusyn software (Version 1.0, ComboSyn Inc., U.S.) based on Chou and Talalay median-effect principle.[36] Combination Index (CI) values of <1, 1, or > 1 are indicative of synergy, additivity, or antagonism respectively. The software also generates CI values at various fractions of cells affected (Fa). The Fa value is proportional to the dose and

therefore Fa vs CI plots can provide the interactive effects of the combinations over the various doses tested. The data, in quadruplicate, is presented as Fa vs CI plots to correlate the effect of the combinations at different treatment concentrations. CI analysis for NP was not conducted as the individual drugs in NP could not be stably produced to directly compare the individual NP and the combination NP groups for interactive effects.

***In vivo assessment of safety and efficacy in  $Tyr\ NRAS^{Q61K}\ RXR\alpha^{L2/L2}$  and  $Tyr\ NRAS^{Q61K}\ RXR^{ep/-}$  metastatic melanoma mouse models***

$Tyr\ NRAS^{Q61K}\ RXR\alpha^{L2/L2}$  (RXR+) and  $Tyr\ NRAS^{Q61K}\ RXR\alpha^{ep/-}$  (RXR-) metastatic melanoma mouse models with the two major mutations (NRAS<sup>Q61K</sup> and RXR $\alpha$ ) found in human melanoma were used for the *in vivo* studies. The generation of  $Tyr\ NRAS^{Q61K}$  mice has been described in detail elsewhere.[8, 11, 12, 33] The mice were housed in ventilated cages with free access to food and water and were maintained at controlled temperature and humidity conditions for the duration of the experiment. Animals that were 8-12 weeks old were sorted into 2 major categories (RXR+ or RXR-). In each category, mice were subdivided into 7 groups with 4 animals per group. The groups included control untreated mice, control empty NP of each charge distribution, and treatment drug loaded NP of each charge distribution for a total of 28 animals per model (n = 56 for both models). Each group, except the untreated group, was treated with empty or three-drug loaded neutral, partially charged, or fully charged NP. Animals were injected SC (every week x 3 cycles) proximal to the inguinal (Figure 11) LN with 150  $\mu$ L/side (total volume 300  $\mu$ L) of the empty or three-drug loaded NP. Based on the drug loading in the nanoparticles, the amount of polymer used, and a dose volume of 300  $\mu$ L per mouse we determined the doses for the three drugs in the treatment group. Thus, each animal received a dose of 20 mg/kg of each drug with a total dose of 60 mg/kg for all three drugs in the treatment groups and the dose of the polymer was approximately 240 mg/kg for all injected NP. During the study (21 days), mice were monitored for signs of acute toxicity such as noticeable changes in general appearance, loss in median body weight  $\geq 15\%$ , or death. On day 21, 7 days post last injection, mice were euthanized and blood samples were collected, centrifuged at 3,000 x g for 7 min and the plasma samples were submitted for complete blood panel chemistry analysis. The analysis was performed at Oregon State University Veterinary Diagnostic Laboratory. The concentrations of blood urea nitrogen (BUN), creatinine, and alanine transaminase (ALT) values were assessed. BUN and creatinine are surrogate markers for kidney toxicity while ALT is a surrogate marker for liver toxicity. [37-39] The quantified values between the treatment and the control groups for both models were compared by one-way ANOVA with Tukey's multiple comparison post-test at a p-value of 0.05 using Graph Pad prism version 5.00 for Windows to assess organ toxicity. Data are presented as mean parameter value  $\pm$  S.D of four replicates.

Immediately post-euthanasia and blood collection the inguinal and axillary LN (Figure 1) were collected and processed immediately to evaluate the efficacy in terms of reduction in

melanocytes in response to the treatment. Briefly, LN were fixed in 4% paraformaldehyde and were embedded in paraffin blocks. For histological studies, 5  $\mu\text{m}$ -thick paraffin sections from mouse LN were rehydrated and Fontana-Masson (FM) staining was performed according to manufacturer's instructions. FM staining of skin-draining LNs is used as a general label for melanin pigment, which represent pigment-producing (melanocytic) cells, the nuclei are stained pink using a secondary Nuclear Red dye for contrast.[40] All microscopic studies were conducted using Leica DME light microscope and analyzed using Leica Application Suite software, version 3.3.1. Images were taken using 20X objective throughout the study. Post staining, quantifications of *melanin-pigmented area* were performed using Adobe Photoshop CS5 software. The pictures of LN were analyzed independently in a double-blind manner by two investigators, and significance was determined using a student's two-tailed unpaired t-test as calculated by Graph Pad Prism software. Data are presented as mean # of melanocytes/pigmented area  $\pm$  SD in inguinal or axillary LN for four replicates.

All animal work was conducted in compliance with NIH guideline and Institutional Animal Care and Use Committee policy at Oregon State University for End-Stage Illness and Pre-emptive Euthanasia based on Humane Endpoints Guidelines.

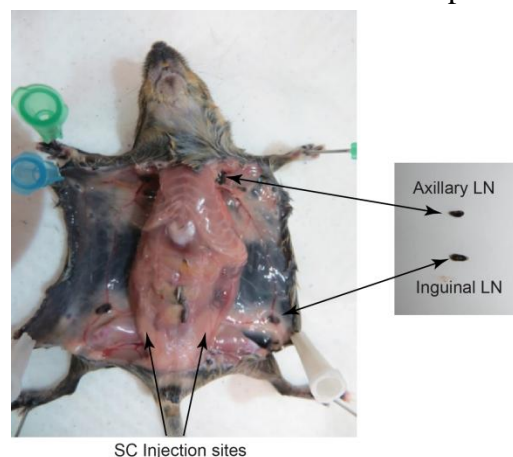


**Figure 1:** Phenotypic appearance of  $Tyr\ NRAS^{Q61K}\ RXR\alpha^{L2/L2}$  (RXR+) or  $Tyr\ NRAS^{Q61K}\ RXR\alpha^{ep-/-}$  (RXR-) with injection site and lymph nodes of interest (Inguinal and Axillary)

## RESULTS AND DISCUSSION

### *Preparation and characterization of three-drug loaded nanoparticles*

Structures for the DTX, EVR, and LY along with a representation of the three-drug loaded NP are depicted in Figure 2. DTX, EVR, and LY neutral, partially charged, and fully charged NP are formulated by varying ratios of mPEG-PCL and COOH-PEG-PCL. Based on the RP-HPLC data the three-drug neutral, partially charged, and fully charged NP are able to solubilize approximately 2 mg of each drug and retain each of the drugs at the initial concentrations (within 6%) for 24 h (Figure 3). The intrinsic aqueous solubilities of DTX, EVR, and LY are 4

$\mu\text{g/mL}$ [26],  $9.6 \mu\text{g/mL}$ [27], and  $243 \mu\text{g/mL}$ [28] respectively. Thus, incorporation of these drugs into the NP increased the solubility of DTX, EVR, and LY by 455 fold, 201 fold and 8 fold respectively, thereby achieving therapeutically relevant dosing concentrations for *in vivo* assessment. Our results are consistent with published results, where the incorporation of hydrophobic drugs into amphiphilic diblock copolymers like PEG-PCL increases their aqueous solubility and stability.[41, 42]

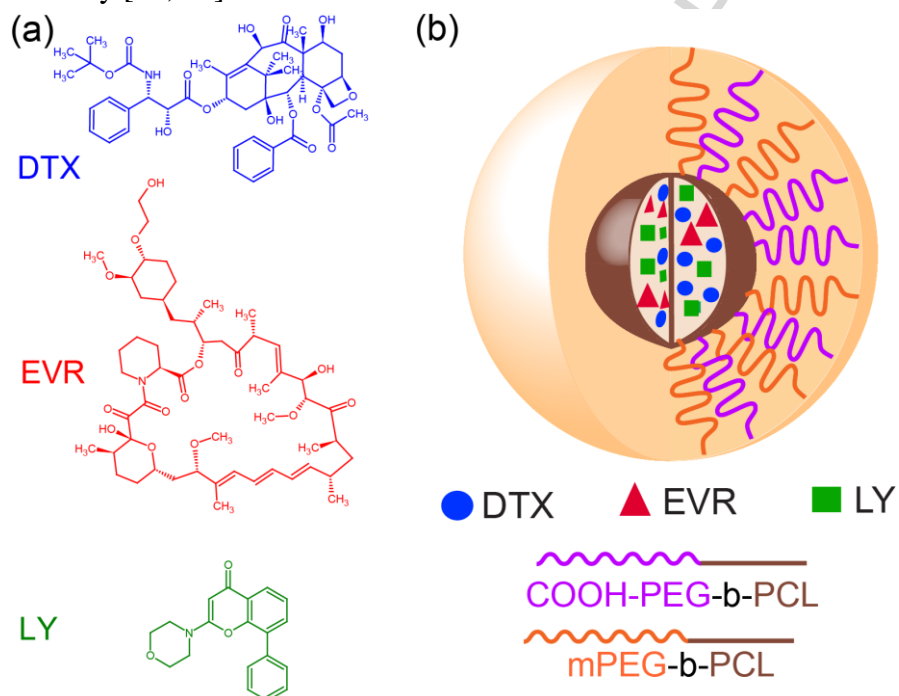


**Figure 2:** Structures of DTX, EVR, and LY (a); Schematic representation of the three-drug (DTX, EVR and LY) loaded NP (b)

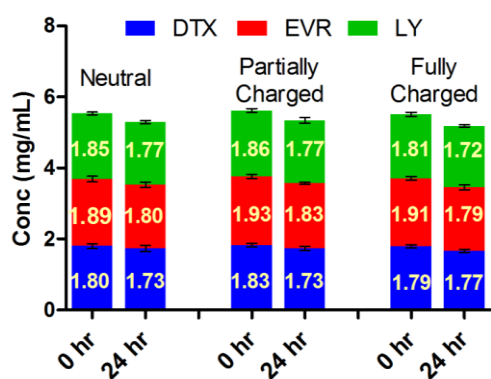


**Figure 3:** Initial loading and drug retention at 24 h for DTX, EVR, and LY in three-drug neutral, partially charged, and fully charged NP (Mean  $\pm$  S.D,  $n = 3$ ). The numbers indicate average loading concentrations for each individual drug in the NP.

The particle sizes and polydispersity index (PDI) for the three-drug neutral, partially charged, and fully charged NP are presented in Table 1. The neutral, partially charged, and fully charged NP show unimodal distribution as indicated with PDI values of less than 0.35. After 24 h under refrigeration and at room temperature, the size was re-assessed and no changes are seen in size or distribution (data not shown). No changes in the size over time are indicative of stability as no aggregation of the NP is occurring. Statistical analysis of the size distribution indicates that there is no significant difference between the particle sizes for neutral, partially charged, and fully charged NP. The mean zeta potential for neutral, partially charged, and fully charged NP are also presented in Table 1. As anticipated, the magnitude of the charge distribution correlates well with the increasing percentage of the negatively charged COOH-PEG-PCL content in the NP.

Size and surface charge are critical parameters in the selective uptake of NP into the lymphatic system.[20] PEG-PCL diblock copolymers can produce NP of uniform size (around 50 nm) that can selectively pass through the gaps in lymphatic endothelium (30-100 nm).[43] Additionally, studies have shown that particles with a size above 20 nm accumulate into the lymphatics, however, when the particle size exceeds 100 nm the rate of particle drainage from the interstitium slows significantly.[20] Thus, optimal particle sizes for interstitial drainage and lymphatic accumulation are between 10 – 80 nm.[2] Accordingly, the drug loaded PEG-PCL NP in our study with an average size of 48 nm are expected to preferentially accumulate into the lymphatics. Surface charge is the other key parameter for lymphatic accumulation.[44] It has been widely reported in the literature that anionic NP have a higher uptake into lymphatic vessels when compared to their neutral and cationic counterparts.[2] Other studies have indicated that highly negative charged particles can trigger macrophage uptake.[45] Therefore, we anticipate that based on the surface charge distribution a differential accumulation of the NP in the lymph nodes *in vivo* will occur. Additionally, as all of the NP have similar sizes any differences in lymphatic uptake can be attributed to the difference in surface charge alone.

|                      | Mean Size $\pm$ SD (nm) | PDI $\pm$ SD    | Mean Zeta Potential ( $\zeta$ ) $\pm$ SD (mV) |
|----------------------|-------------------------|-----------------|---|
| Neutral NP           | 48.08 $\pm$ 0.31        | 0.31 $\pm$ 0.01 | -6.4 $\pm$ 0.24                               |
| Partially charged NP | 48.30 $\pm$ 0.42        | 0.25 $\pm$ 0.01 | -19.2 $\pm$ 2.15                              |
| Fully charged NP     | 48.60 $\pm$ 0.66        | 0.31 $\pm$ 0.02 | -37.6 $\pm$ 1.02                              |

**Table 1:** Particle Size, PDI, and Zeta potential values for three-drug neutral, partially charged and fully charged NP (Mean  $\pm$  SD, n = 3)

### ***In vitro* drug release from the nanoparticles**

The release profiles of DTX, EVR and LY from the three-drug neutral, partially charged, and fully charged NP at pH 5.0 and 7.4 are shown in Figure 4 and the final % drug released values are presented in Table 2 ..

| Drug | % Drug Released at 168 h |              |                      |              |                  |              |
|------|--------------------------|--------------|----------------------|--------------|------------------|--------------|
|      | Neutral NP               |              | Partially Charged NP |              | Fully Charged NP |              |
|      | pH 5.0                   | pH 7.4       | pH 5.0               | pH 7.4       | pH 5.0           | pH 7.4       |
| DTX  | 72.00 ± 2.16             | 72.42 ± 2.66 | 68.55 ± 0.43         | 75.01 ± 1.78 | 69.80 ± 1.07     | 73.60 ± 1.82 |
| EVR  | 44.58 ± 1.61             | 51.67 ± 5.83 | 46.23 ± 0.85         | 58.23 ± 2.18 | 48.19 ± 2.85     | 61.38 ± 4.67 |
| LY   | 81.18 ± 1.22             | 81.60 ± 1.39 | 80.12 ± 1.42         | 81.90 ± 0.67 | 80.33 ± 0.52     | 81.24 ± 2.07 |

**Table 2:** The % drug released values for DTX, EVR, and LY in neutral, partially charged, and fully charged NP at pH 5.0 and 7.4 over 168 h. Data presented is Mean ± SD (n = 3)

The highest % release occurred with LY, followed by DTX, and then EVR. Overall, there is no significant difference in the rates of drug release for each drug from NP of different compositions at the same pH (Table 2 and Figure 4). The release profile of DTX, EVR and LY from the neutral, partially charged, and fully charged NP was almost identical at both pHs and exhibited no statistically significant difference (Table 2). The two phase exponential association  $t_{1/2}$  and  $r^2$  values for DTX, EVR, and LY release from the neutral, partially, and fully charged NP are presented in Table 3. However, the fast and slow half-lives were longer at pH 7.4 as compared to pH 5 as expected due to the higher rate of ester hydrolysis of the PEG-PCL at the lower pH. As seen in Figure 4, there is an initial phase involving burst/rapid release of the drugs from the NP followed by a more sustained release pattern at later stages. This biphasic release pattern exhibited by PEG-PCL NP has been well documented in the literature.[46, 47] The initial burst release is primarily driven by the desorption and the diffusion of surface adsorbed drug particles, while the secondary phase of drug release is driven by the erosion of the NP matrix and drug diffusion processes. The inner segment, PCL, is a biodegradable polyester that has a high crystallinity while the outer PEG shell increases the porosity in the PCL matrix and thereby allows the diffusion of drugs from the matrix into the buffer.[48] Thus drug release is governed by diffusion of the drug and erosion/degradation of the NP matrix.[49] Previous studies have demonstrated that solid state interactions between the drug and the hydrophobic block, and the mobility of the hydrophobic block all govern the drug release rate.[46] LY has the fastest drug release from the three-drug NP followed by DTX and then EVR. This may be due to the relative hydrophobicities of these molecules and their potential interaction with the PCL domain. The log D values at pH 7.4 for LY, DTX and EVR are 3.33, 3.54, and 4.25 respectively (Advanced Chemistry Development ACD/Universal LogD Module, Percepta 14.0.0 (Build 1996)).

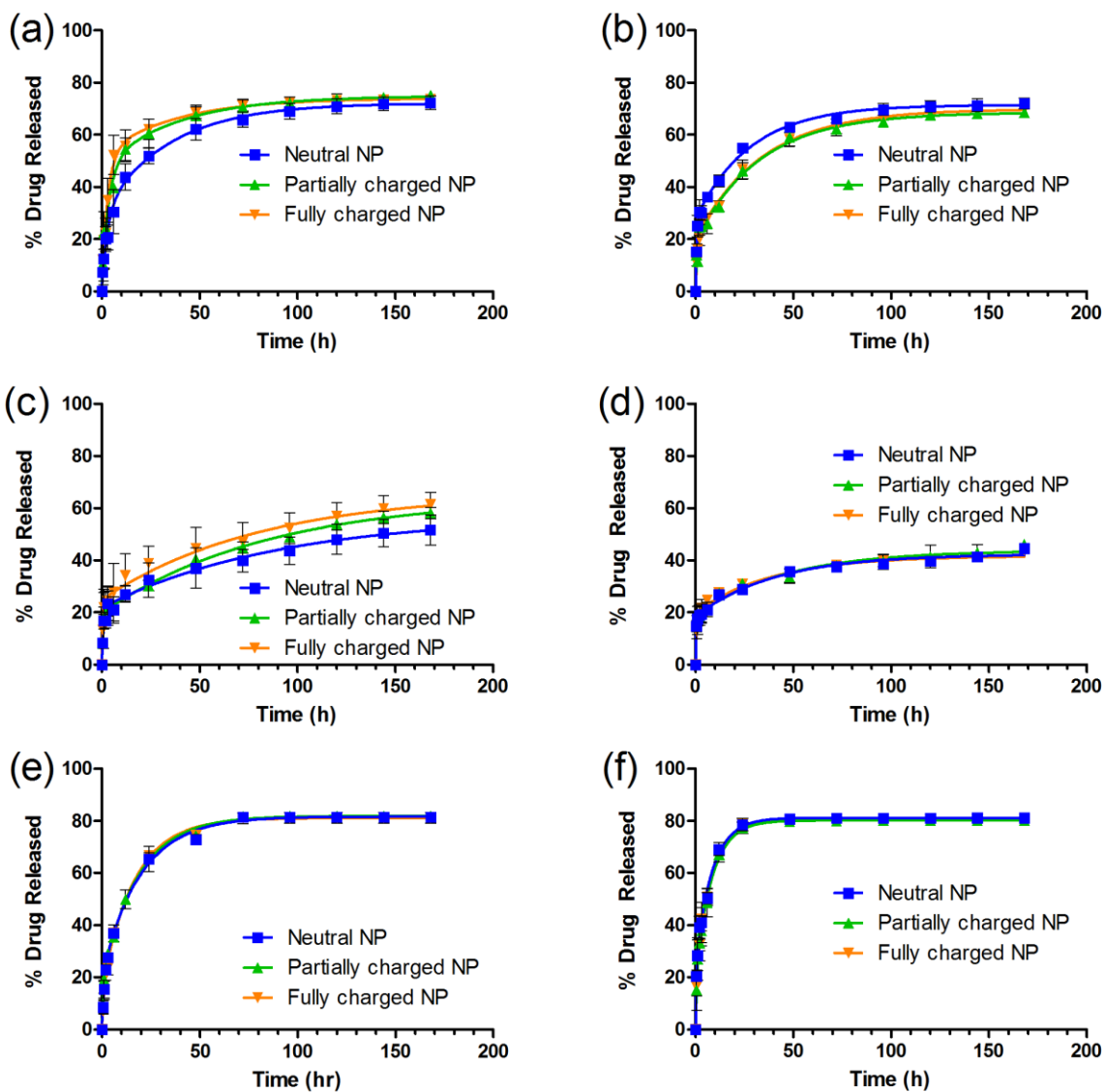


**Figure 4:** *In vitro* drug release profiles of DTX at pH 7.4 (a) and pH 5.0 (b), EVR at pH 7.4 (c) and pH 5.0 (d), and LY at pH 7.4 (e) and pH 5.0 (f) from neutral, partially charged, and fully charged NP under sink conditions over 48 h. (Mean % drug release  $\pm$  S.D, n = 3)

| NP                   | Drug | pH 5.0             |                    |        | pH 7.4             |                    |        |
|----------------------|------|--------------------|--------------------|--------|--------------------|--------------------|--------|
|                      |      | Fast $t_{1/2}$ (h) | Slow $t_{1/2}$ (h) | $r^2$  | Fast $t_{1/2}$ (h) | Slow $t_{1/2}$ (h) | $r^2$  |
| Neutral NP           | DTX  | 0.42               | 19.49              | 0.9924 | 2.05               | 23.93              | 0.9817 |
|                      | EVR  | 0.23               | 28.25              | 0.9822 | 0.61               | 63.20              | 0.9099 |
|                      | LY   | 0.31               | 5.93               | 0.9902 | 0.83               | 13.72              | 0.9957 |
| Partially charged NP | DTX  | 0.42               | 22.75              | 0.9865 | 2.46               | 26.84              | 0.9816 |
|                      | EVR  | 0.21               | 31.17              | 0.9644 | 0.51               | 59.53              | 0.9843 |
|                      | LY   | 0.33               | 5.93               | 0.9803 | 0.50               | 12.83              | 0.9964 |
| Fully charged NP     | DTX  | 0.53               | 23.73              | 0.9936 | 2.10               | 25.90              | 0.9600 |
|                      | EVR  | 0.39               | 27.03              | 0.9717 | 0.45               | 56.38              | 0.9226 |
|                      | LY   | 0.38               | 5.44               | 0.9945 | 0.70               | 11.41              | 0.9955 |

**Table 3:** Fast and slow half-lives ( $t_{1/2}$ ) and goodness of fit ( $r^2$ ) values of DTX, EVR, and LY in neutral, partially charged, and fully charged NP at pH 5.0 and 7.4 using a two phase association curve fitting.

#### *In vitro cell viability assay and combination index (CI) analysis*

The anti-proliferative effects ( $IC_{50}$  values) of DTX, EVR, and LY in DMSO individually and in two- and three-drug combinations evaluated in A375 human melanoma cells are presented in Figure 5(a). The two-drug combinations and the three-drug combinations in DMSO exhibited strong inhibition of A375 cell proliferation over a wide range of tested doses. Based on the data (Figure 5(a)) the two- and three- drug combinations are more potent as compared to the individual drug treatments, with the three-drug combination demonstrating the highest potency at 0.57 nM concentration. The two- and three- drug combinations were also evaluated for interactive effects (synergistic, additive, or antagonistic) using Compusyn software and the data are presented in Figure 5(b). The two-drug combination EVR:LY is synergistic at lower concentrations but becomes additive at higher concentrations. The DTX:EVR and DTX:LY combinations are synergistic at all concentrations (Figure 5(b)). The three-drug combination is also synergistic at all the fractions affected indicating that the multiple mechanisms of action enhance the potency of the combination beyond what is expected with individual drug treatments alone. The combination neutral, partially charged, and fully charged NP were also evaluated for their respective  $IC_{50}$  values and data is presented in Figure 5(c). Not surprisingly the NP have a higher  $IC_{50}$  values as compared to the drugs/combinations in DMSO. This is due to the fact that the drug must not undergo diffusion from the NP and release is also dependent on the degradation of the NP. Additionally, the cell culture conditions do not mimic the sink conditions one can expect *in vivo* further slowing down the rate of drug release from the NP. Our findings

are consistent with other published studies documenting the same phenomena.[50, 51] The empty NP did not affect cell viability (data not shown). CI analysis for NP was not feasible as the individual drugs in NP could not be stably produced to directly compare the individual NP and the combination NP groups for interactive effects.

The two-drug combinations, DTX:EVR and DTX:LY, illustrate the need to target multiple pathways, such as microtubule stabilization and mTOR inhibition. Interestingly, with EVR:LY, which specifically targets mTOR1 and mTOR2, at higher concentrations A375 cells seem to be able to overcome the synergy of this one pathway and maybe up/down regulating others and becoming less susceptible to drug(s) effects. Not surprisingly, the three-drug combination achieves sustained synergistic effects at the highest potency by blocking multiple pathways involved in cancer progression. Cancer cells up regulate alternative mechanisms to induce drug resistance when one particular pathway is blocked.[52] The mTOR pathway is involved in cell growth, proliferation, and survival, and in addition it affects downstream effector proteins which are essential for the protein translation processes.[52] It has been reported previously that the mTOR pathway is highly up regulated in malignant melanoma due to the NRAS mutation [53] and inhibiting the mTOR pathway can have beneficial effects in the treatment regimen.[54] EVR acts on the mTOR1 pathway and it is known that the cancer cells immediately up regulate the mTOR2 pathway to induce drug resistance when the mTOR1 pathway is blocked.[55] LY targets the mTOR2 pathway and also blocks the PI3K/AKT pathway. Thus, when LY is used in combination with EVR, the mTOR cascade is completely blocked.[54] Ablation of RXR $\alpha$  alongside with NRAS<sup>Q61K</sup> mutations results in an increased number/size of spontaneous melanomas with reduced latency and increased invasion to draining lymph nodes in the NRAS<sup>Q61K</sup> | RXR $\alpha$ <sup>ep/-</sup> mice).[15] Thus, far there are no drugs targeting this mutation specifically. Therefore, the three drug combination was evaluated in both the RXR+ and RXR- mice to determine the efficacy of the regimen in both. DTX acts by a completely different mechanism where it stabilizes the microtubules and thereby induces apoptosis as a general chemotherapeutic strategy.[56] Thus, the combination of these three drugs can synergistically inhibit proliferation through multiple mechanisms of action as evidenced by the potency and CI for the three-drug combination as compared to individual drugs or the two-drug combinations.

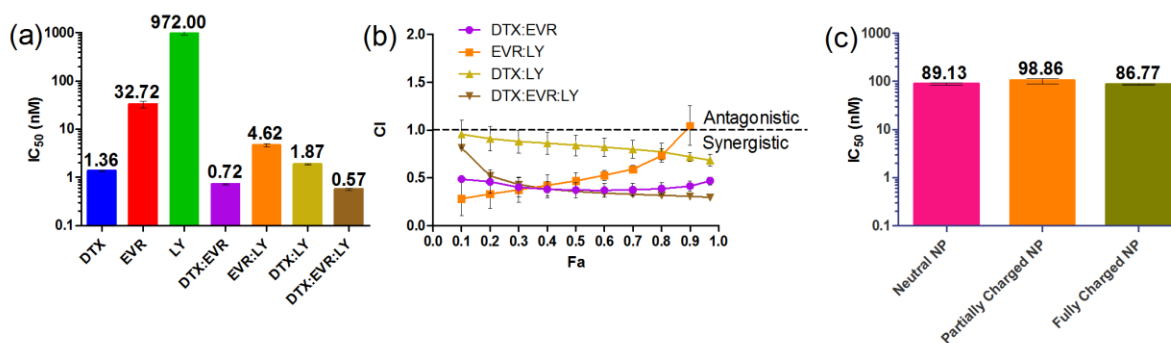


**Figure 5:** Mean IC<sub>50</sub> values of DTX, EVR, LY, two- and three-drug combinations in DMSO in A375 metastatic melanoma cells (n = 4) (a). Fa vs CI plot of the two- and three- drug combinations in A375 metastatic melanoma cells (n = 4) (b). Mean IC<sub>50</sub> values of three-drug combination neutral, partially charged and fully charged nanoparticles in A375 metastatic melanoma cells (n = 4) (c)

***In vivo assessment of safety and efficacy in  $Tyr\ NRAS^{Q61K}\ RXR\alpha^{L2/L2}$  and  $Tyr\ NRAS^{Q61K}\ RXR\alpha^{ep-/-}$  metastatic melanoma mouse models***

The safety profile of the neutral, partially charged, and fully charged NP has been evaluated in two metastatic melanoma mouse models containing activating  $NRAS^{Q61K}$  driver mutation and with or without  $RXR\alpha$  protein ( $RXR+$  or  $RXR-$ ), which develop melanoma with different latency and with LN metastasis as described elsewhere.[15] None of the mice in either model died or exhibited abnormal behavioral changes during the duration of the study. Changes in the weight, during the course of the study, for the neutral, partially charged, and fully charged NP, with or without the three drugs are presented in Figure 6. Based on the data, none of the groups in either model demonstrated weight loss  $\geq 15\%$  indicating that neither the empty NP nor the three-drug NPs produce acute toxicity at 20 mg/kg dose of each drug (total 60 mg/kg dose) and 240 mg/kg of the NP polymer.

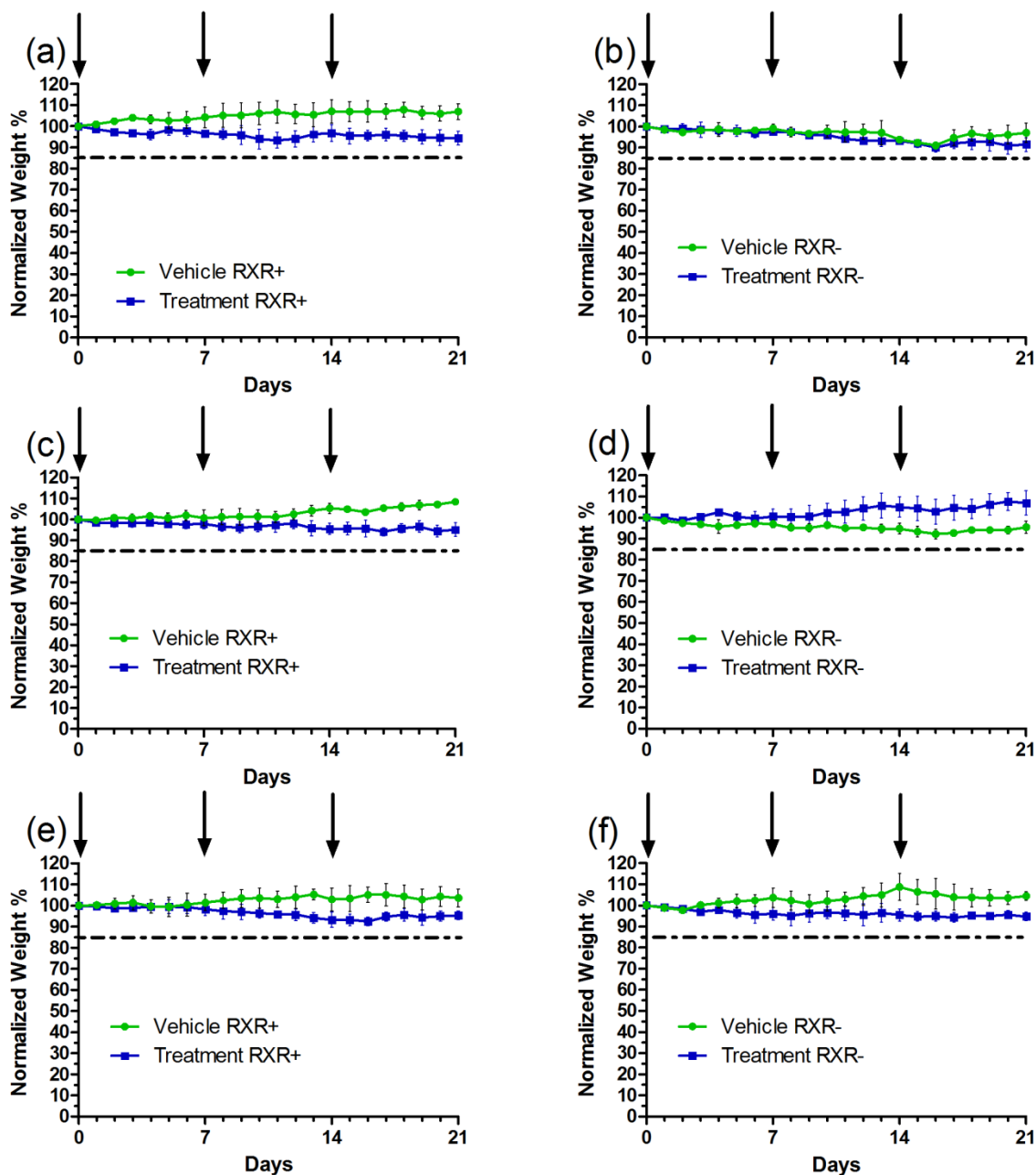


**Figure 6:** Normalized body weight of mice injected subcutaneously with empty or three drug NP in Tyr Nras<sup>Q61K</sup> RXR $\alpha$ <sup>L2/L2</sup> (RXR+) (a, c, and e) and Tyr Nras<sup>Q61K</sup> RXR $\alpha$ <sup>ep-/-</sup> (RXR-) (b, d, and f) mice. Neutral NP in RXR+ (a) and RXR- (b), partially charged NP in RXR+ (c) and RXR- (d) mice, and fully charged NP in RXR+ (e) and RXR- (f) mice. The mice were injected at a dose of 20 mg/kg for each drug in the treatment group and 240 mg/kg of the polymer in all groups. The arrows indicate the days of injection (0, 7, 14). The dashed line depicts the threshold weight loss of 15% which is indicative of acute toxicity. (Mean normalized weight %  $\pm$  S.D, n=4).

The blood biochemical values for BUN, Creatinine, and ALT, for all the groups in each model are presented in Figures 7 – 9. BUN, Creatinine, and ALT values in RXR+ and RXR- treated with empty neutral or three-drug neutral NP indicates that there are no statistically significant differences between the treatment groups and the untreated and vehicle controls (Figure 7). Similar results were seen with the partially charged (Figure 8) and fully charged (Figure 9) NP groups. BUN, and creatinine levels are indicators of kidney function.[38] In cases of renal toxicity, levels of BUN and/or creatinine are elevated.[38] ALT is present in all tissues throughout the entire body, but is particularly concentrated in liver, bile duct, kidney, and bone.[39] Elevated ALT levels are usually indicative of liver toxicity.[39] Based on the behavioral observations, weight data (Figure 5), and the biochemical estimations (Figure 7 – 9) no acute toxicity is observed with either the empty or three-drug loaded NP.

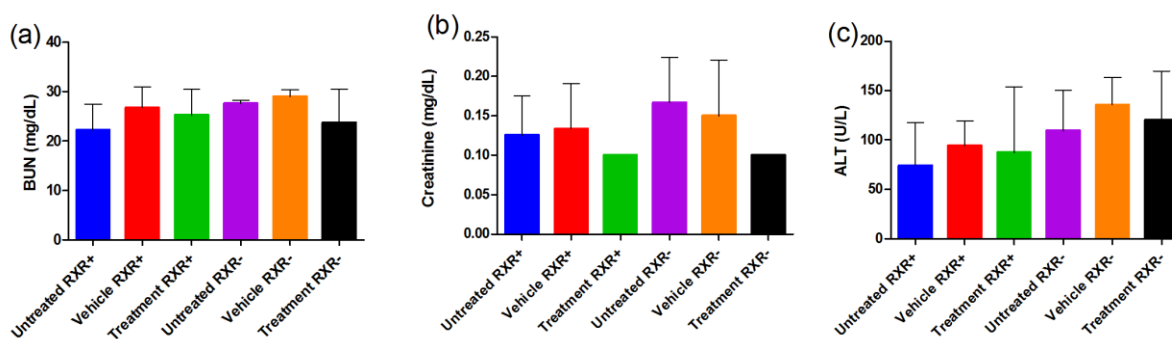


**Figure 7:** Blood panel data from mice injected subcutaneously with vehicle (empty neutral NP) or treatment (three-drug neutral NP) in *Tyr NRAS<sup>Q61K</sup> RXR $\alpha$ <sup>L2/L2</sup>* (RXR+) and *Tyr NRAS<sup>Q61K</sup> RXR $\alpha$ <sup>pp/-</sup>* (RXR-) mice. BUN (a), Creatinine (b), and ALT (c). Mean parameter value  $\pm$  S.D, n=4. One way ANOVA with Tukey's Multiple Comparison test was used for statistical analysis at p-value of 0.05

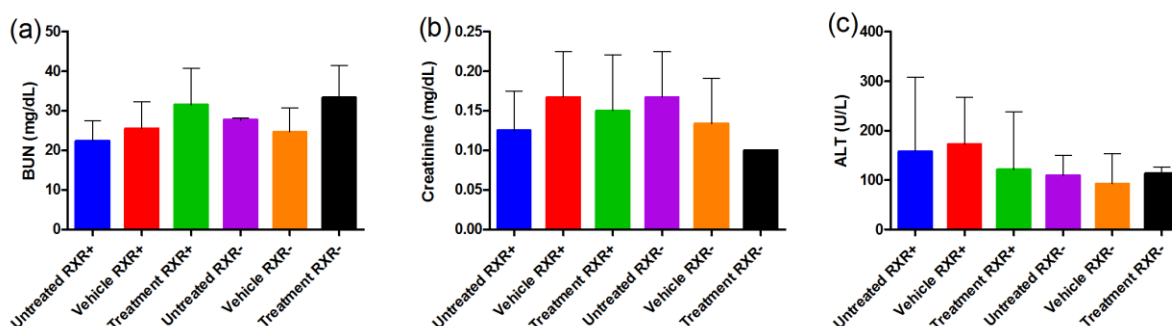


**Figure 8:** Blood panel data from mice injected subcutaneously with vehicle (empty partially charged NP) or treatment (three-drug partially charged NP) in *Tyr NRAS<sup>Q61K</sup> RXR $\alpha$ <sup>L2/L2</sup>* (RXR+) and *Tyr NRAS<sup>Q61K</sup> RXR $\alpha$ <sup>pp/-</sup>* (RXR-) mice. BUN (a), Creatinine (b), and ALT (c). Mean

parameter value  $\pm$  S.D, n=4. One way ANOVA with Tukey's Multiple Comparison test was used for statistical analysis at p-value of 0.05

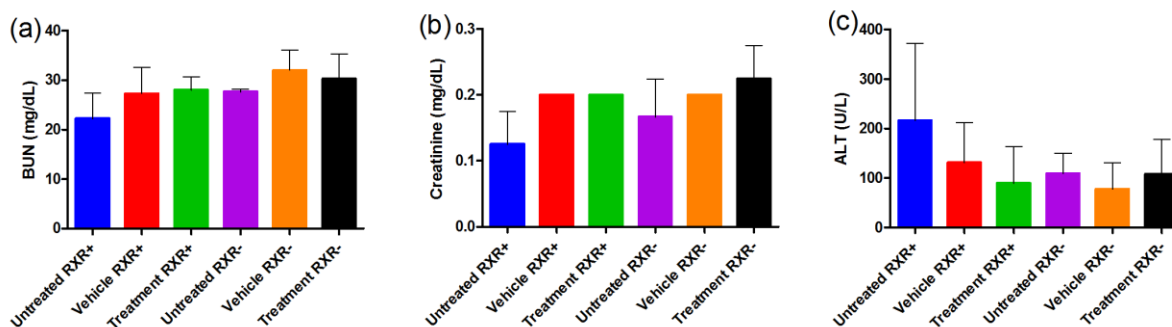


**Figure 9:** Blood panel data from mice injected subcutaneously with vehicle (empty fully charged NP) or treatment (three-drug fully charged NP) in *Tyr NRAS<sup>Q61K</sup> RXR $\alpha$ <sup>L2/L2</sup>* (RXR+) and *Tyr NRAS<sup>Q61K</sup> RXR $\alpha$ <sup>ep-/-</sup>* (RXR-) mice. BUN (a), Creatinine (b), and ALT (c). Mean parameter value  $\pm$  S.D, n=4. One way ANOVA with Tukey's Multiple Comparison test was used for statistical analysis at p-value of 0.05

The effectiveness of the treatment in the two different models of metastatic melanoma mouse models is established using Fontana Masson (FM) staining of the LN followed by quantification of pigment areas covered with invading melanocytes in the draining LN using Adobe Photoshop CS5 software. The melanocyte covered pigmented area (black stain) between the empty NP and the three-drug NP for the same charge distribution were compared to quantify the efficacy, in terms of decrease in the number of invasive, malignant melanocytes in the LNs.

A representative microscopic data set from the inguinal and axillary LN is presented in Figure 9 for RXR+ and RXR- mice treated with neutral, partially charged, and fully charged empty or three-drug NP. The reduction in the transformed melanocytes covered pigmented area is dependent on the uptake and trafficking of the differently charged NP in the lymphatic system. As seen in figure 10(a), with three-drug neutral NP as compared to empty neutral NP a reduction in melanocytes area in the inguinal LN (proximal to the injection sites) is seen in both models (RXR+ and RXR-), however, no change in pigmented melanocytes area was noted in the axillary LN (distal from the injection sites). Thus, indicating that the efficacy of the drug loaded neutral particles is limited to the inguinal LN in both models. Analysis of melanocyte covered pigmented area indicates a statistically significant difference ( $p = 0.0003$ ) at the inguinal LN of both the RXR+ and RXR- groups (Figure 11 (a & b)), but no difference is observed at the axillary LN. One possible explanation is that the NP remained at the site of injection after dosing and showed efficacy only at the proximal inguinal LN. One of the ways by which particles traffic into the lymphatic system is through charge repulsion between the NP and the interstitium at the site of injection.[44] For the neutral NP the magnitude of the surface charge may not be large enough to induce electrostatic repulsions to allow for distal trafficking through the lymphatics. Additionally, studies by others have shown that neutral NP tend to aggregate at the site of

injection which may also confirm our findings that the particles do not track distally into the lymphatics but show efficacy regionally.[57]

In comparing the three-drug partially charged NP to empty partially charged NP (Figure 10(b)), a decrease in melanocytes at both the inguinal and the axillary LN in both models is noted. These results indicate that the three-drug partially charged NP are efficacious at both the proximal (inguinal) and distal (axillary) LN as referenced from the site of injection for both the models. Analysis of melanocyte covered pigmented area indicates a statistically significant difference at both the inguinal ( $p < 0.0001$ ) and the axillary ( $p < 0.0001$ ) LN in both the mouse models upon treatment with the three-drug partially charged NP (Figure 11(c & d)). The lymphatic vessels and the interstitium have a slight negative charge because of the presence of glycosaminoglycans and the electrostatic repulsions between these and the partially charged NP (surface charge of -19 mV) may be responsible for the deeper movement of the particles into the lymphatic system.[44] The ability of these NP to track into the distal LN may provide an excellent opportunity to target advanced stages of metastatic melanoma and improve patient outcomes.

Comparing the staining in empty fully charged and three-drug fully charged NP (Figure 10(c)), no difference at either the inguinal or the axillary LN is observed in both models. Thus, establishing that the fully charged NP did not have appreciable accumulation in either of the two LN studied. Analysis of melanocyte covered pigmented area indicates no difference between empty and three-drug fully charged NP at both the inguinal and axillary LN in both models (Figure 11(e & f)). The data indicates that highly negatively charged particles did not tract into either the regional or distal LN (Figure 10c, 11e & f). Previously published literature has suggested that highly negatively charged particles are rapidly taken up and sequestered by macrophages.[45] The high anionic charge on these NP also tends to attract serum proteins resulting in the formation of a protein corona that promotes the release of signals for macrophage uptake.[45] For example, anionic polystyrene nanoparticles have 4 times higher uptake by macrophages in serum as compared to uptake from buffer solutions indicting the role of serum proteins in the uptake mechanism and kinetics.[45] Research has also indicated that highly anionic nanoparticles resemble bacteria in their surface charge and therefore interact preferentially with phagocytic cells.[58] Additional studies in the future to characterize the immune responses triggered by the different NPs may shed light about the involvement of immune cells, including the macrophages, in the lymphatic tracking of these NP.

We have used two different animal models in this study containing mutations in NRAS and/or RXR $\alpha$  to elucidate the effectiveness of our developed drug delivery system and to characterize the efficacy and toxicity of our formulated NP.[4-8, 11] The *Tyr NRAS<sup>Q61K</sup> RXR $\alpha$ <sup>L2/L2</sup>* (RXR+) mice represent a model with increased latency to develop invasive melanoma while *Tyr NRAS<sup>Q61K</sup> RXR $\alpha$ <sup>pp/-</sup>* (RXR-) bigenic mice, selectively lacking RXR $\alpha$  in the epidermis alongside with the activating NRAS mutation in the melanocytes, represent a metastatic melanoma model

where melanoma cells readily migrate and invade the lymphatics.[9, 33] Analysis of melanocyte covered pigmented area comparing RXR+ and RXR- for the three-drug NP with same charge distribution indicates that no statistically significant difference is demonstrated (Figures 10 & 11). Thereby indicating that the NP retained efficacy across the two different melanoma models. Future studies using fluorescent dye loaded NP will be performed to obtain further insight about the biodistribution of these NP while simultaneously tracking their lymphatic movement and accumulation.

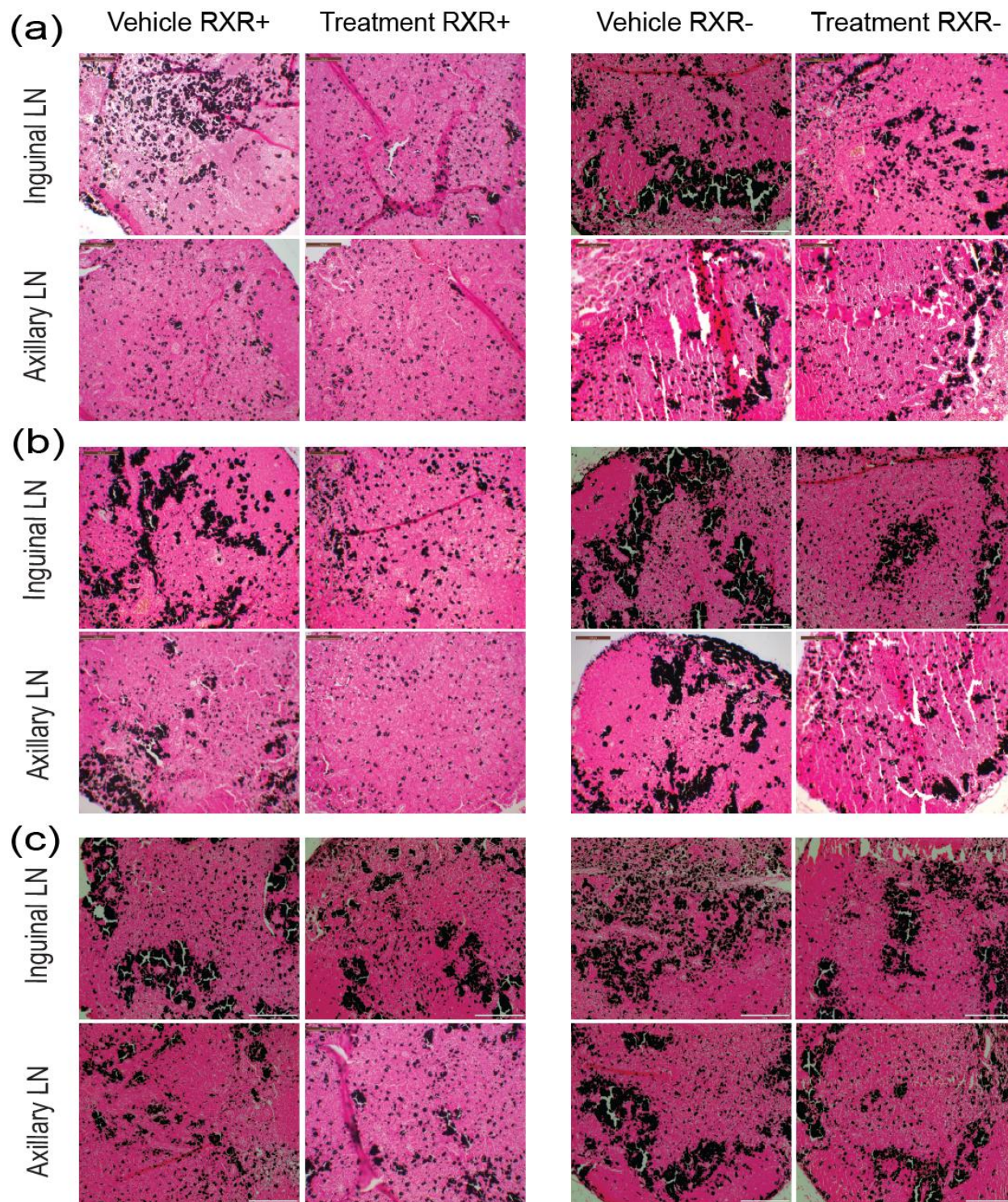


**Figure 10:** Representative pictures of FM staining of LN sections after treatment with vehicle (empty NP) or treatment (three-drug NP) in *Tyr NRAS<sup>Q61K</sup> RXR $\alpha$ <sup>L2/L2</sup>* (RXR+) and *Tyr NRAS<sup>Q61K</sup> RXR $\alpha$ <sup>ep/-</sup>* (RXR-) mice. Neutral NP in RXR+ and RXR- mice (a), partially charged NP in RXR+ and RXR- mice (b), and fully charged NP in RXR+ and RXR- mice (c). The mice were injected at a dose of 20 mg/kg for each drug in the treatment group and 240 mg/kg of the polymer in all groups on days 0, 7, and 14. Scale bar: 100  $\mu$ m (n = 4)

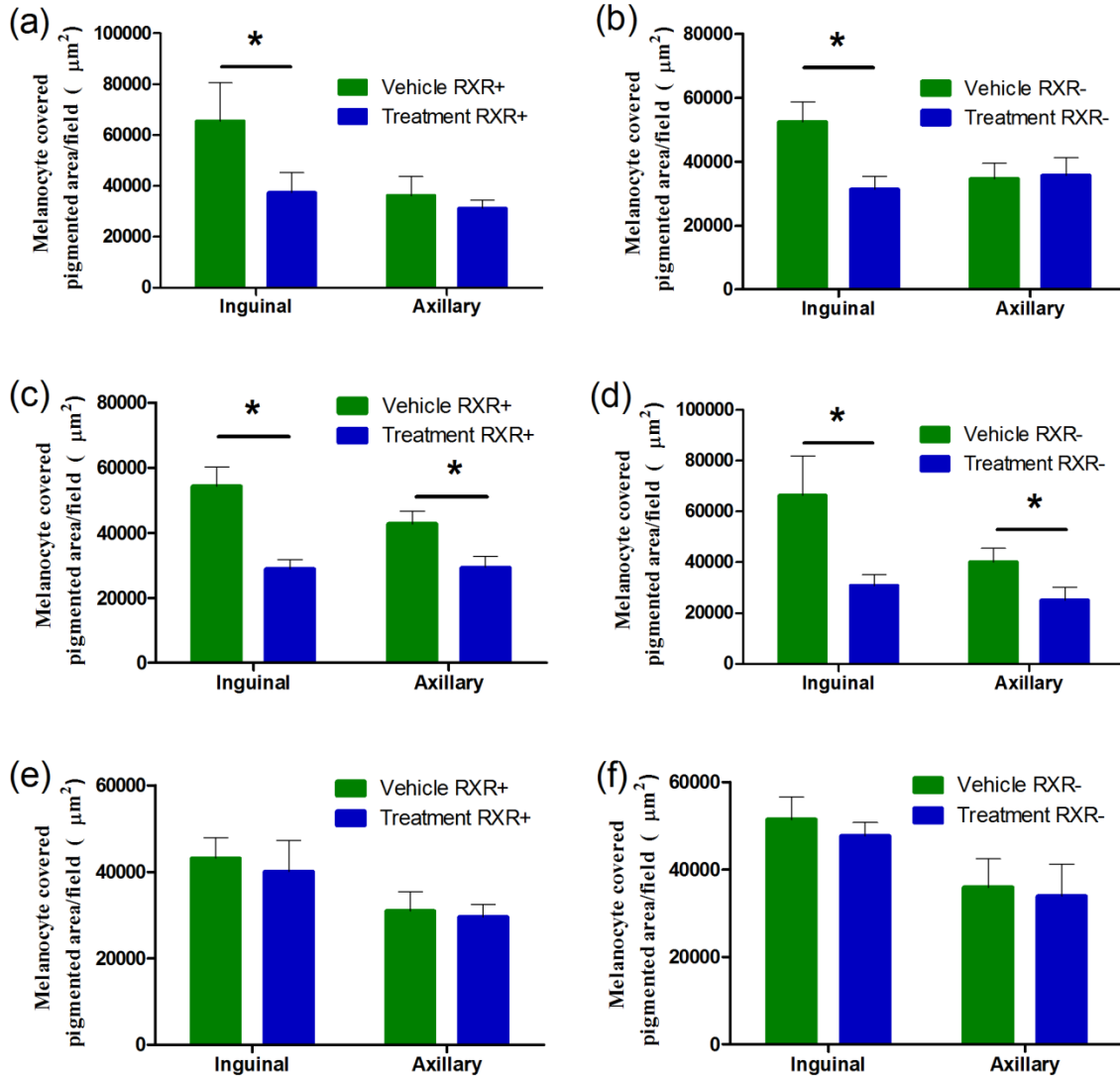


**Figure 11:** Mean melanocytic pigmented area per field ( $\mu\text{m}^2$ ) treated with empty or three-drug NP in *Tyr NRAS<sup>Q61K</sup> RXR $\alpha$ <sup>L2/L2</sup>* (RXR+) and *Tyr NRAS<sup>Q61K</sup> RXR $\alpha$ <sup>ep/-</sup>* (RXR-) negative mice. Neutral NP in RXR+ (a) and RXR- (b) mice, partially charged NP in RXR+ (c) and RXR- (d) mice, fully charged NP in RXR+ (e) and RXR- (f) mice. The mice were injected at a dose of 20 mg/kg for each drug in the treatment group and 240 mg/kg of the polymer in all groups on days

0, 7, and 14. Values are expressed as a mean  $\pm$  SEM (n =4). \*indicates statistical significance as determined by a Student's two-tailed unpaired t-test with a p-value of 0.05

## CONCLUSION

In summary, we have developed and characterized a three-drug (DTX, EVR and LY) NP that acts synergistically *in vivo* in two different melanoma mouse models. Our results indicate that the effect of the three-drug neutral NP is proximal to the site of injection, while the three-drug partially charged NP track further into the lymphatic system reaching more distal LNs. In contrast, the three-drug fully charged NP have minimal effects on the proximal or distal LN. The three-drug combination neutral and partially charged NP are highly effective in treating melanoma in both models and provide the basis for a novel therapeutic option treating metastatic melanoma that is targeted to the site of action, i.e. the lymphatic system.

## ACKNOWLEDGEMENTS

This study was supported by Oregon State University-Startup fund.

## References

- [1] J.A. Lo, D.E. Fisher, The melanoma revolution: from UV carcinogenesis to a new era in therapeutics. *Science* 346(6212) (2014) 945-949. 10.1126/science.1253735
- [2] G.M. Ryan, L.M. Kaminskas, C.J. Porter, Nano-chemotherapeutics: maximising lymphatic drug exposure to improve the treatment of lymph-metastatic cancers. *J Control Release* 193 (2014) 241-256. 10.1016/j.jconrel.2014.04.051
- [3] A. Alitalo, M. Detmar, Interaction of tumor cells and lymphatic vessels in cancer progression. *Oncogene* 31(42) (2012) 4499-4508. 10.1038/onc.2011.602
- [4] I.C. Glitza, M.A. Davies, Genotyping of cutaneous melanoma. *Chin Clin Oncol* 3(3) (2014) 27. 10.3978/j.issn.2304-3865.2014.03.01
- [5] M. Pracht, A. Mogha, A. Lespagnol, A. Fautrel, N. Mouchet, F. Le Gall, V. Paumier, C. Lefeuvre-Plesse, N. Rioux-Leclerc, J. Mosser, E. Oger, H. Adamski, M.D. Galibert, T. Lesimple, Prognostic and predictive values of oncogenic BRAF, NRAS, c-KIT and MITF in cutaneous and mucous melanoma. *J Eur Acad Dermatol Venereol* 29(8) (2015) 1530-1538. 10.1111/jdv.12910
- [6] A.K. Eisfeld, S. Schwind, K.W. Hoag, C.J. Walker, S. Liyanarachchi, R. Patel, X. Huang, J. Markowitz, W. Duan, G.A. Otterson, W.E. Carson, 3rd, G. Marcucci, C.D. Bloomfield, A. de la Chapelle, NRAS isoforms differentially affect downstream pathways, cell growth, and cell transformation. *Proc Natl Acad Sci U S A* 111(11) (2014) 4179-4184. 10.1073/pnas.1401727111
- [7] Z. Wang, D.J. Coleman, G. Bajaj, X. Liang, G. Ganguli-Indra, A.K. Indra, RXRalpha ablation in epidermal keratinocytes enhances UVR-induced DNA damage, apoptosis, and proliferation of keratinocytes and melanocytes. *J Invest Dermatol* 131(1) (2011) 177-187. 10.1038/jid.2010.290

- [8] D.J. Coleman, G. Garcia, S. Hyter, H.S. Jang, S. Chagani, X. Liang, L. Larue, G. Ganguli-Indra, A.K. Indra, Retinoid-X-receptors (alpha/beta) in melanocytes modulate innate immune responses and differentially regulate cell survival following UV irradiation. *PLoS Genet* 10(5) (2014) e1004321. 10.1371/journal.pgen.1004321
- [9] M. Mandala, B. Merelli, D. Massi, Nras in melanoma: targeting the undruggable target. *Crit Rev Oncol Hematol* 92(2) (2014) 107-122. 10.1016/j.critrevonc.2014.05.005
- [10] K. Omholt, S. Karsberg, A. Platz, L. Kanter, U. Ringborg, J. Hansson, Screening of N-ras codon 61 mutations in paired primary and metastatic cutaneous melanomas: mutations occur early and persist throughout tumor progression. *Clin Cancer Res* 8(11) (2002) 3468-3474.
- [11] J. Ackermann, M. Frutschi, K. Kaloulis, T. McKee, A. Trumpp, F. Beermann, Metastasizing melanoma formation caused by expression of activated N-RasQ61K on an INK4a-deficient background. *Cancer Res* 65(10) (2005) 4005-4011. 10.1158/0008-5472.CAN-04-2970
- [12] L. Mansi, E. Viel, E. Curtit, J. Medioni, C. Le Tourneau, [Targeting the RAS signalling pathway in cancer]. *Bull Cancer* 98(9) (2011) 1019-1028. 10.1684/bdc.2011.1380
- [13] V.J. Mar, W. Liu, B. Devitt, S.Q. Wong, A. Dobrovic, G.A. McArthur, R. Wolfe, J.W. Kelly, The role of BRAF mutations in primary melanoma growth rate and survival. *Br J Dermatol* 173(1) (2015) 76-82. 10.1111/bjd.13756
- [14] S. Hyter, G. Bajaj, X. Liang, M. Barbacid, G. Ganguli-Indra, A.K. Indra, Loss of nuclear receptor RXRalpha in epidermal keratinocytes promotes the formation of Cdk4-activated invasive melanomas. *Pigment Cell Melanoma Res* 23(5) (2010) 635-648. 10.1111/j.1755-148X.2010.00732.x
- [15] D.J. Coleman, S. Chagani, S. Hyter, A.M. Sherman, C.V. Lohr, X. Liang, G. Ganguli-Indra, A.K. Indra, Loss of keratinocytic RXRalpha combined with activated CDK4 or oncogenic NRAS generates UVB-induced melanomas via loss of p53 and PTEN in the tumor microenvironment. *Mol Cancer Res* 13(1) (2015) 186-196. 10.1158/1541-7786.MCR-14-0164
- [16] A. Marzuka, L. Huang, N. Theodosakis, M. Bosenberg, Melanoma Treatments: Advances and Mechanisms. *J Cell Physiol* 230(11) (2015) 2626-2633. 10.1002/jcp.25019
- [17] C. Karimkhani, R. Gonzalez, R.P. Dellavalle, A review of novel therapies for melanoma. *Am J Clin Dermatol* 15(4) (2014) 323-337. 10.1007/s40257-014-0083-7
- [18] M.S. Soengas, S.W. Lowe, Apoptosis and melanoma chemoresistance. *Oncogene* 22(20) (2003) 3138-3151. 10.1038/sj.onc.1206454
- [19] D.A. Rao, M.L. Forrest, A.W. Alani, G.S. Kwon, J.R. Robinson, Biodegradable PLGA based nanoparticles for sustained regional lymphatic drug delivery. *J Pharm Sci* 99(4) (2010) 2018-2031. 10.1002/jps.21970

- [20] A. Ali Khan, J. Mudassir, N. Mohtar, Y. Darwis, Advanced drug delivery to the lymphatic system: lipid-based nanoformulations. *Int J Nanomedicine* 8 (2013) 2733-2744. 10.2147/IJN.S41521
- [21] A. Supersaxo, W.R. Hein, H. Steffen, Effect of molecular weight on the lymphatic absorption of water-soluble compounds following subcutaneous administration. *Pharm Res* 7(2) (1990) 167-169.
- [22] Y. Xie, T.R. Bagby, M.S. Cohen, M.L. Forrest, Drug delivery to the lymphatic system: importance in future cancer diagnosis and therapies. *Expert Opin Drug Deliv* 6(8) (2009) 785-792. 10.1517/17425240903085128
- [23] D.N. McLennan, C.J. Porter, S.A. Charman, Subcutaneous drug delivery and the role of the lymphatics. *Drug Discov Today Technol* 2(1) (2005) 89-96. 10.1016/j.ddtec.2005.05.006
- [24] J. Kota, K.K. Machavaram, D.N. McLennan, G.A. Edwards, C.J. Porter, S.A. Charman, Lymphatic absorption of subcutaneously administered proteins: influence of different injection sites on the absorption of darbepoetin alfa using a sheep model. *Drug Metab Dispos* 35(12) (2007) 2211-2217. 10.1124/dmd.107.015669
- [25] K.D. Wilson, S.G. Raney, L. Sekirov, G. Chikh, S.D. deJong, P.R. Cullis, Y.K. Tam, Effects of intravenous and subcutaneous administration on the pharmacokinetics, biodistribution, cellular uptake and immunostimulatory activity of CpG ODN encapsulated in liposomal nanoparticles. *Int Immunopharmacol* 7(8) (2007) 1064-1075. 10.1016/j.intimp.2007.04.002
- [26] S. Mazzaferro, K. Bouchemal, J.F. Gallard, B.I. Iorga, M. Cheron, C. Gueutin, C. Steinmesse, G. Ponchel, Bivalent sequential binding of docetaxel to methyl-beta-cyclodextrin. *Int J Pharm* 416(1) (2011) 171-180. 10.1016/j.ijpharm.2011.06.034
- [27] Y. Iwase, Y. Maitani, Preparation and in vivo evaluation of liposomal everolimus for lung carcinoma and thyroid carcinoma. *Biol Pharm Bull* 35(6) (2012) 975-979.
- [28] W. Saiyin, D. Wang, L. Li, L. Zhu, B. Liu, L. Sheng, Y. Li, B. Zhu, L. Mao, G. Li, X. Zhu, Sequential release of autophagy inhibitor and chemotherapeutic drug with polymeric delivery system for oral squamous cell carcinoma therapy. *Mol Pharm* 11(5) (2014) 1662-1675. 10.1021/mp5000423
- [29] J.M. Chan, P.M. Valencia, L. Zhang, R. Langer, O.C. Farokhzad, Polymeric nanoparticles for drug delivery. *Methods Mol Biol* 624 (2010) 163-175. 10.1007/978-1-60761-609-2\_11
- [30] K. Letchford, H. Burt, A review of the formation and classification of amphiphilic block copolymer nanoparticulate structures: micelles, nanospheres, nanocapsules and polymersomes. *Eur J Pharm Biopharm* 65(3) (2007) 259-269. 10.1016/j.ejpb.2006.11.009
- [31] N. Dubey, R. Varshney, J. Shukla, A. Ganeshpurkar, P.P. Hazari, G.P. Bandopadhaya, A.K. Mishra, P. Trivedi, Synthesis and evaluation of biodegradable PCL/PEG nanoparticles for

neuroendocrine tumor targeted delivery of somatostatin analog. *Drug Deliv* 19(3) (2012) 132-142. 10.3109/10717544.2012.657718

[32] X. He, L. Li, H. Su, D. Zhou, H. Song, L. Wang, X. Jiang, Poly(ethylene glycol)-block-poly(epsilon-caprolactone)-and phospholipid-based stealth nanoparticles with enhanced therapeutic efficacy on murine breast cancer by improved intracellular drug delivery. *Int J Nanomedicine* 10 (2015) 1791-1804. 10.2147/IJN.S75186

[33] M. Li, H. Chiba, X. Warot, N. Messaddeq, C. Gerard, P. Chambon, D. Metzger, RXR-alpha ablation in skin keratinocytes results in alopecia and epidermal alterations. *Development* 128(5) (2001) 675-688.

[34] H.R. Marsden, L. Gabrielli, A. Kros, Rapid preparation of polymersomes by a water addition/solvent evaporation method. *Polymer Chemistry* 1(9) (2010) 1512-1518. 10.1039/c0py00172d

[35] J. Shen, D.J. Burgess, Dissolution Testing Strategies for Nanoparticulate Drug Delivery Systems: Recent Developments and Challenges. *Drug Deliv Transl Res* 3(5) (2013) 409-415. 10.1007/s13346-013-0129-z

[36] T.C. Chou, P. Talalay, Quantitative analysis of dose-effect relationships: the combined effects of multiple drugs or enzyme inhibitors. *Adv Enzyme Regul* 22 (1984) 27-55.

[37] S.M. DeAtley, M.Y. Aksenov, M.V. Aksenova, B. Jordan, J.M. Carney, D.A. Butterfield, Adriamycin-induced changes of creatine kinase activity in vivo and in cardiomyocyte culture. *Toxicology* 134(1) (1999) 51-62.

[38] A. Jamshidzadeh, R. Heidari, S. Mohammadi-Samani, N. Azarpira, A. Najbi, P. Jahani, N. Abdoli, A comparison between the nephrotoxic profile of gentamicin and gentamicin nanoparticles in mice. *J Biochem Mol Toxicol* 29(2) (2015) 57-62. 10.1002/jbt.21667

[39] S.P. Singh, M. Kumari, S.I. Kumari, M.F. Rahman, M. Mahboob, P. Grover, Toxicity assessment of manganese oxide micro and nanoparticles in Wistar rats after 28 days of repeated oral exposure. *J Appl Toxicol* 33(10) (2013) 1165-1179. 10.1002/jat.2887

[40] V.S. Carriel, J. Aneiros-Fernandez, S. Arias-Santiago, I.J. Garzon, M. Alaminos, A. Campos, A novel histochemical method for a simultaneous staining of melanin and collagen fibers. *J Histochem Cytochem* 59(3) (2011) 270-277. 10.1369/0022155410398001

[41] X. Wei, C. Gong, M. Gou, S. Fu, Q. Guo, S. Shi, F. Luo, G. Guo, L. Qiu, Z. Qian, Biodegradable poly(epsilon-caprolactone)-poly(ethylene glycol) copolymers as drug delivery system. *Int J Pharm* 381(1) (2009) 1-18. 10.1016/j.ijpharm.2009.07.033

[42] S.R. Mudshinge, A.B. Deore, S. Patil, C.M. Bhalgat, Nanoparticles: Emerging carriers for drug delivery. *Saudi Pharm J* 19(3) (2011) 129-141. 10.1016/j.jsps.2011.04.001

- [43] G. Luo, X. Yu, C. Jin, F. Yang, D. Fu, J. Long, J. Xu, C. Zhan, W. Lu, LyP-1-conjugated nanoparticles for targeting drug delivery to lymphatic metastatic tumors. *Int J Pharm* 385(1-2) (2010) 150-156. 10.1016/j.ijpharm.2009.10.014
- [44] S.T. Proulx, P. Luciani, L.C. Dieterich, S. Karaman, J.C. Leroux, M. Detmar, Expansion of the lymphatic vasculature in cancer and inflammation: new opportunities for in vivo imaging and drug delivery. *J Control Release* 172(2) (2013) 550-557. 10.1016/j.jconrel.2013.04.027
- [45] O. Lunov, T. Syrovets, C. Loos, J. Beil, M. Delacher, K. Tron, G.U. Nienhaus, A. Musyanovych, V. Mailander, K. Landfester, T. Simmet, Differential uptake of functionalized polystyrene nanoparticles by human macrophages and a monocytic cell line. *ACS Nano* 5(3) (2011) 1657-1669. 10.1021/nn2000756
- [46] W. Peng, X.Y. Jiang, Y. Zhu, E. Omari-Siaw, W.W. Deng, J.N. Yu, X.M. Xu, W.M. Zhang, Oral delivery of capsaicin using MPEG-PCL nanoparticles. *Acta Pharmacol Sin* 36(1) (2015) 139-148. 10.1038/aps.2014.113
- [47] R. Li, X. Li, L. Xie, D. Ding, Y. Hu, X. Qian, L. Yu, Y. Ding, X. Jiang, B. Liu, Preparation and evaluation of PEG-PCL nanoparticles for local tetradrine delivery. *Int J Pharm* 379(1) (2009) 158-166. 10.1016/j.ijpharm.2009.06.007
- [48] F. Ahmed, D.E. Discher, Self-porating polymersomes of PEG-PLA and PEG-PCL: hydrolysis-triggered controlled release vesicles. *J Control Release* 96(1) (2004) 37-53. 10.1016/j.jconrel.2003.12.021
- [49] P.R. Lockman, R.J. Mumper, M.A. Khan, D.D. Allen, Nanoparticle technology for drug delivery across the blood-brain barrier. *Drug Dev Ind Pharm* 28(1) (2002) 1-13. 10.1081/DDC-120001481
- [50] X. Cheng, L. Kuhn, Chemotherapy drug delivery from calcium phosphate nanoparticles. *Int J Nanomedicine* 2(4) (2007) 667-674.
- [51] X. Xu, C.R. Sabanayagam, D.A. Harrington, M.C. Farach-Carson, X. Jia, A hydrogel-based tumor model for the evaluation of nanoparticle-based cancer therapeutics. *Biomaterials* 35(10) (2014) 3319-3330. 10.1016/j.biomaterials.2013.12.080
- [52] R. Marone, D. Erhart, A.C. Mertz, T. Bohnacker, C. Schnell, V. Cmiljanovic, F. Stauffer, C. Garcia-Echeverria, B. Giese, S.M. Maira, M.P. Wymann, Targeting melanoma with dual phosphoinositide 3-kinase/mammalian target of rapamycin inhibitors. *Mol Cancer Res* 7(4) (2009) 601-613. 10.1158/1541-7786.MCR-08-0366
- [53] C. Posch, H. Moslehi, L. Feeney, G.A. Green, A. Ebaee, V. Feichtenschlager, K. Chong, L. Peng, M.T. Dimon, T. Phillips, A.I. Daud, T.H. McCalmont, P.E. LeBoit, S. Ortiz-Urda, Combined targeting of MEK and PI3K/mTOR effector pathways is necessary to effectively inhibit NRAS mutant melanoma in vitro and in vivo. *Proc Natl Acad Sci U S A* 110(10) (2013) 4015-4020. 10.1073/pnas.1216013110

- [54] M. Karbowniczek, C.S. Spittle, T. Morrison, H. Wu, E.P. Henske, mTOR is activated in the majority of malignant melanomas. *J Invest Dermatol* 128(4) (2008) 980-987. 10.1038/sj.jid.5701074
- [55] W.J. Oh, E. Jacinto, mTOR complex 2 signaling and functions. *Cell Cycle* 10(14) (2011) 2305-2316.
- [56] M. Joerger, Metabolism of the taxanes including nab-paclitaxel. *Expert Opin Drug Metab Toxicol* 11(5) (2015) 691-702. 10.1517/17425255.2015.983074
- [57] M.P. Osborne, V.J. Richardson, K. Jeyasingh, B.E. Ryman, Radionuclide-labelled liposomes--a new lymph node imaging agent. *Int J Nucl Med Biol* 6(2) (1979) 75-83.
- [58] E. Frohlich, The role of surface charge in cellular uptake and cytotoxicity of medical nanoparticles. *Int J Nanomedicine* 7 (2012) 5577-5591. 10.2147/IJN.S36111